Available online at www.sciencedirect.com

SCIENCE DIRECT®

International Journal of Coal Geology 59 (2004) 245–271

International Journal of COAL GEOLOGY

www.elsevier.com/locate/ijcoalgeo

Application of SAXS and SANS in evaluation of porosity, pore size distribution and surface area of coal

A.P. Radlinski[a], M. Mastalerz[b,*], A.L. Hinde[a], M. Hainbuchner[c], H. Rauch[c], M. Baron[d], J.S. Lin[e], L. Fan[f], P. Thiyagarajan[f]

[a] *Geoscience Australia, Canberra, Australian Capital Territory, Australia*
[b] *Indiana Geological Survey, Indiana University, 611 North Walnut Grove, Bloomington, IN, USA*
[c] *Atominstitut der Österreichischen Universitäten, Vienna, Austria*
[d] *Institute Max von Laue—Paul Langevin, Grenoble, France*
[e] *Oak Ridge National Laboratory, Oak Ridge, TN, USA*
[f] *Argonne National Laboratory, Argonne, IL, USA*

Received 29 October 2003; accepted 4 March 2004
Available online 15 June 2004

Abstract

This paper discusses the applicability of small angle X-ray scattering (SAXS) and small angle neutron scattering (SANS) techniques for determining the porosity, pore size distribution and internal specific surface area in coals. The method is noninvasive, fast, inexpensive and does not require complex sample preparation. It uses coal grains of about 0.8 mm size mounted in standard pellets as used for petrographic studies.

Assuming spherical pore geometry, the scattering data are converted into the pore size distribution in the size range 1 nm (10 Å) to 20 μm (200,000 Å) in diameter, accounting for both open and closed pores. FTIR as well as SAXS and SANS data for seven samples of oriented whole coals and corresponding pellets with vitrinite reflectance (R_o) values in the range 0.55% to 5.15% are presented and analyzed. Our results demonstrate that pellets adequately represent the average microstructure of coal samples.

The scattering data have been used to calculate the maximum surface area available for methane adsorption. Total porosity as percentage of sample volume is calculated and compared with worldwide trends. By demonstrating the applicability of SAXS and SANS techniques to determine the porosity, pore size distribution and surface area in coals, we provide a new and efficient tool, which can be used for any type of coal sample, from a thin slice to a representative sample of a thick seam.

Keywords: SAXS; SANS; Porosity; Pore size distribution; Surface area; Coal

1. Introduction

The geometry of pore space (pore size distribution and total porosity) and the specific surface area are important characteristics of coal as they have profound influence on the behavior of coal as a reservoir rock for gas. Together with gas-specific sorption

* Corresponding author. Tel.: +1-812-855-9416; fax: +1-812-855-2862.
E-mail address: mmastale@indiana.edu (M. Mastalerz).

0166-5162/$ - see front matter © 2004 Elsevier B.V. All rights reserved.
doi:10.1016/j.coal.2004.03.002

characteristics (Yee et al., 1993), these parameters control adsorption capacity for gases such as methane and carbon dioxide (Bustin and Clarkson, 1998; Crosdale et al., 1998). Because of that, the pore size distribution and specific surface area are major parameters to be determined in order to understand (1) coalbed methane desorption and extraction, and (2) CO_2 sorption into coal for carbon sequestration purposes (Clarkson and Bustin, 2000; Gentzis, 2000).

Various methods have been used to study the microstructure of coals, in particular, the pore size distribution and surface area. Mercury injection and nitrogen adsorption are commonly used to quantify these parameters. Results for any particular coal, however, vary depending upon the fluid probe used, which reflects both the specificity of sorption phenomena as well as a degree of modification of the coal microstructure when in contact with various sorbates like water, carbon dioxide, methane or nitrogen (Levine, 1993). Other techniques used to characterize porosity and pore size distribution include SEM, TEM, small angle scattering of X-rays (SAXS) and neutrons (SANS).

SAXS and SANS permit detection of a wide range of pore sizes in a single experimental run. These techniques have been applied relatively recently to systematic studies of organic matter of geological origin, and they show a lot of promise both for research on coal (Radlinski and Radlinska, 1999; Radlinski et al., 2001; Boreham et al., 2003) and kerogen (Radlinski et al., 2000a,b; Radlinski and Hinde, 2001, 2002). The coal samples used in initial studies were in the form of solid platelets cut out parallel to the bedding plane (Radlinski and Radlinska, 1999). Such an orientation was chosen to avoid anisotropy that could render data interpretation difficult. From the point of view of applied coal research, however, orientation parallel to the bedding plane is not very practical because it gives characteristics of only one or, at best, some of the macerals present in the coal. In contrast to this, a pellet sample allows macerals of all orientations and from different coal beds to be averaged. Hence, data obtained from pellet samples provide the pore size distribution representative of the whole coal, such as a coal bench or coal seam, which is the microstructural information needed to determine, for example, the coalbed methane adsorption capacity or CO_2 adsorption capacity. Although SAXS or SANS do not actually measure the amount of CH_4 or CO_2 adsorbed by the coal, they directly and noninvasively measure the internal surface area available for sorption of fluids of various molecular sizes.

As demonstrated in our preliminary study, in order for the scattering techniques to yield a pore size distribution representative of the coal seam (or a desired part of it), they should be adapted to analyze a representative crushed coal sample (Radlinski et al., 2001). This requires experiments to be performed on representative pellet samples. Furthermore, a range of solid (oriented) and pellet coal samples of different rank must be analyzed in order to determine to what extent the anisotropy of coal sample influences the scattering signal and how, in turn, this influences the computed pore size distribution. The purpose of this study is to address these issues and to show that SAXS and SANS can be used to reliably determine the pore size distribution in coals.

2. Background of SAXS and SANS

SAXS and SANS have been used for decades to study the geometry of supramolecular objects. These objects can be suspended in solvents or aggregated into a solid phase. With a modern small angle scattering

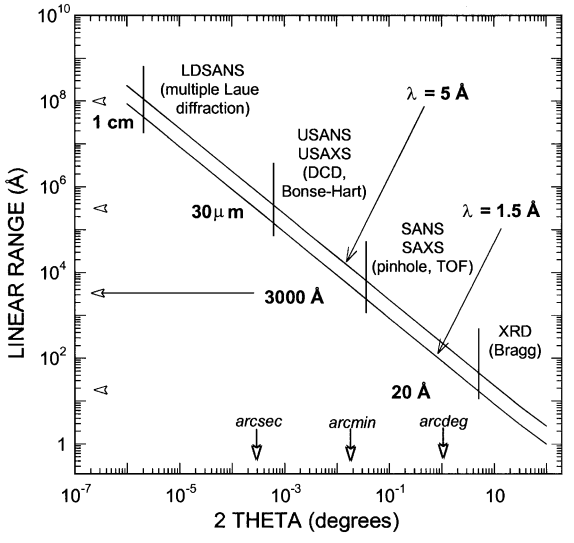

Fig. 1. Range of linear sizes of pores that can be observed with various types of neutron and X-ray optics. Solid lines delineate the region of typical radiation wavelengths used in experimental practice.

apparatus, the size of objects accessible with SAXS and SANS extends from about 1 nm (10 Å) to about 20 μm (200,000 Å; Fig. 1). There is an extensive literature about the theory and practice of small angle scattering (for a review, see Guinier et al., 1955; Espinat, 1990; Lindner and Zemb, 1991), including its applications to sedimentary rocks and coal (Radlinski and Radlinska, 1999; Radlinski et al., 1996, 1999, 2000a,b, 2001; Radlinski and Hinde, 2001, 2002; Lin et al., 1978; Bale and Schmidt, 1984; Wong et al., 1986; Mildner and Hall, 1986; Winans and Thiyagarajan, 1988; Cody et al., 1997). SAXS and SANS are attractive alternatives to using fluids for probing the pore space. The scattering techniques are inexpensive, noninvasive, require little sample preparation and can be performed both on oriented whole coal samples and standard crushed pellets.

Scattering of X-rays or neutrons occurs because of the scattering contrast between various components within the medium. X-rays probe the fluctuations of the electronic density, whereas neutrons probe the fluctuations of the nuclear scattering cross section (Radlinski and Hinde, 2001, 2002). In general, these fluctuations reflect the chemical heterogeneity and density variations within the sample. In particular, the pore space in coal has high contrast with the coal matrix for both X-rays and neutrons.

In small angle scattering experiments, a beam of thermal neutrons or X-rays of fixed wavelength and known intensity is incident on a highly transmitting sample under investigation, and the intensity of scattered radiation is measured versus the (small) scattering angle, i.e., looking almost directly into the transmitted beam. Information pertinent to the size distribution of scattering objects can be retrieved from the scattering intensity, traditionally plotted versus the scattering vector, Q: $Q=(4\pi/\lambda)\sin(\Theta/2)$, where Θ is the scattering angle and λ is the wavelength of X-rays or neutrons. In the small angle scattering regime, Θ does not exceed 5°, therefore $\sin(\Theta/2) \sim \Theta/2$, and Q is just the scattering angle expressed in different units ($Å^{-1}$ instead of degrees). The intensity of scattered radiation (X-rays or neutrons) is routinely calibrated against a laboratory scattering standard, thus providing means to calculate the absolute scattering cross section for every coal sample. In a nutshell, the absolute scattering cross section is the intensity scattered at a given angle Θ by a 100% transparent sample of a unit volume, provided the incident beam has a unit intensity. This is a very useful concept, as it enables testing of theoretical predictions as well as direct comparisons between various samples. In this work, the plots of "scattering intensity" actually show the absolute scattering cross sections in units of cm^{-1}.

For scattering objects of roughly spherical geometry (i.e., pores or foreign inclusions in sedimentary rocks), the dominant contribution to the scattering intensity, measured at a particular value of Q, comes from scattering objects within the linear size range $2.5/Q +/- 50\%$ (Radlinski et al., 2000a,b). In order to enable studies of objects of various sizes and various contrast values, SAXS and SANS instruments are designed with a view to maximizing the Q-range and minimizing various parasitic contributions to the scattering signal.

In order to resolve the scattering signal from the transmitted (central) beam, two major optical designs are used: pinhole geometry and double crystal spectrometer geometry, the latter also known as Bonse–Hart camera (Bonse and Hart, 1965). These two types of instruments are usually referred to as small-angle scattering SAXS (or SANS) and ultrasmall angle scattering USAXS (or USANS) machines.

Pinhole geometry machines are typically employed for measurements at scattering angles larger than several minutes of arc and less than about 5° of arc, which corresponds to a scattering object size range of 1 to 300 nm. In pinhole geometry, the SAS signal is resolved from the transmitted beam by collimating the incident beam with a series of slits, moving the detector away from the sample and using a central beam stop to block the transmitted beam.

For the ultrasmall angle region, with scattering angles in the range from about 1 arcsec to 1 arcmin and the corresponding linear size range 300 nm to 30 μm, the resolution of the transmitted and scattered beam is achieved by collimating and analyzing the beam using multiple reflections from perfect silicon crystals (Lambard and Zemb, 1991; Agamalian et al., 1997). Practical USANS machines were developed only recently, and they proved very useful for microstructural studies of geological materials (Radlinski et al., 2001, 1999; Radlinski and Hinde, 2001, 2002).

For homogeneous media, the scattering of X-rays or neutrons occurs exclusively on the interface between the solid matrix and the pore space. For coal, sorbates like water, CO_2, CH_4, N_2 and other fluids, can interact with coal matrix that may lead to microstructural modifications manifested as swelling. In this work, we perform measurements on resin-fixed pellets and our results pertain to coal microstructure in this particular environment. In general, it is feasible to perform SAXS and SANS studies on coal saturated with various sorbates and then conjecture both about the mechanisms of sorption and the microstructural modification of coal matrix by sorbents. An example of such work in a related field (water sorption in sandstones) is given in Broseta et al. (2001).

The pattern of scattered intensity versus scattering angle is determined by the geometry of the pore–matrix interface at various length scales. This can be translated into a pore size distribution if the shape of individual pores is known or can be reasonably assumed. For the results to be quantitative, one needs to know the elemental composition and specific density of the solid matrix in order to calculate the absolute scattering power for X-rays or neutrons.

Coals are chemically heterogeneous from seam scale to molecular scale. The scattering contrast between pore environment and coal matrix, however, is large compared to variations within the matrix itself. The interpretation of SAS data for coal depends critically on the homogeneity of the coal matrix as perceived by the type of radiation used. The most favorable situation arises when the coal matrix is perceived as fully homogeneous on all length scales, which leads to a single contrast value between the solid coal and the pore space. Calculations show that, for coals, such a situation is often observed for the scattering of thermal neutrons, as (1) the scattering powers (technically called the scattering length density, SLD) for various macerals are similar to each other and depend only weakly on the coal rank, and (2) maceral SLDs are also similar to those characteristic of typical ash (Radlinski and Hinde, 2001, 2002). Consequently, the coal matrix (with mineral matter inclusions) is perceived by thermal neutrons as a nearly homogeneous mass. For X-rays, however, the organic matrix, ash and voids are perceived as three separate phases. Such scattering characteristics of neutrons and X-rays enormously reduce the complexity of a geopolymeric system that encompasses the full range of organic materials comprising coal to a relatively simple solid matrix—pore space representation for neutrons, or coal matrix—mineral intrusions—pore space representation for X-rays.

3. Techniques

From each coal, two coal fractions were analyzed: hand-picked vitrain and whole coal. From each fraction, three samples were prepared: one sample cut parallel to the bedding, one sample perpendicular to the bedding and one representative sample crushed to a grain diameter of about 0.8 mm (similar to standard petrographic pellets). This paper will concentrate on the whole coal samples.

Ultimate analysis of the coal samples followed standard ASTM procedure (ASTM, 1985). For petrographic analysis, coal samples were mounted into polished blocks and polished according to standard procedures (Bustin et al., 1985). Maceral analysis and vitrinite reflectance were determined using a Zeiss Photoscope microscope.

Samples for infrared analyzes were prepared using the standard potassium bromide (KBr) pellet method. Pellets were analyzed on a Nicolet 20SXC spectrometer equipped with a DTGS detector collecting 1024 scans per sample at a resolution of 4 cm^{-1}. Bands were identified by comparison with published assignments. Aromaticity ratio was calculated by dividing intergrated areas of aromatic bands in the 3000–3100 cm^{-1} region by aliphatic bands in the 2800–3000 cm^{-1} region. Surface area of coal was determined by N_2 adsorption by Marc Bustin, utilizing single-point surface area, BET surface area and Langmuir surface area plots.

In this work, we used the 10 m SAXS instrument at the Oak Ridge National Laboratory (Russell et al., 1988) and the SANS instrument SAND at the Intense Pulsed Neutron Source, Argonne National Laboratory (Thiyagarayan et al., 1998). The 10 m SAXS instrument is a pinhole-geometry machine equipped with a rotating anode Cu Kα source and a position-sensitive area detector. The SAND instru-

ment is a time-of-flight machine, which uses a wide bandwidth of neutrons with wavelengths 1–14 Å, a large position-sensitive area detector and a wide-angle bank of detectors at fixed distances from the sample. The combination of wide bandwidth of neutrons and position-sensitive detectors that can extend measurements to a scattering angle of $\Theta = 35°$ covers a Q-range of 0.004 to 4 $Å^{-1}$ in a single measurement. Both SAXS and SANS data were acquired and processed in a way that obtains the scattering cross section in absolute units of cm^{-1}. USANS data were obtained with instrument S18 at the High Flux Reactor in Grenoble (Hainbuchner et al., 2000). These data were reduced to pinhole geometry using standard techniques (Hinde, in press).

4. Characteristics of the coals

A set of seven Carboniferous coal samples from the Illinois basin and the Appalachian basin with vitrinite reflectance of 0.55% to 5.15% (from high volatile bituminous to anthracite rank) was selected for this study (Table 1). The coal samples have a wide range of ash content (from 2.35% in Elk Run to 16.44% in FGT-221) and sulfur content (from 0.4% to 3.92%; Fig. 2). Carbon content varies from about 66.74% (dry) in two FGT samples to 92.75% (dry) in the anthracite, and the correlation between R_o and carbon (dry ash free) content follows the well-established trend for coals (Fig. 3; Berkowitz, 1979). There is a good correlation between the vitrinite reflectance (R_o) and the corresponding hydrogen-to-carbon ratio (Fig. 4).

Petrographic composition of the coals varies. High volatile bituminous coals (FGT-6 221 and FGT-6 460.65) have relatively low liptinite content and variable vitrinite and inertinite content (Fig. 5). Elk Run and Herndon samples are similar with regard to petrographic composition, whereas Bolt, Ammonate and anthracite lack liptinite macerals and are composed of vitrinite and varying proportions of inertinite (Fig. 5).

FTIR provides information about the evolution, with increasing rank, of functional groups in the coal samples studied. FTIR spectra of kerogen from coal with R_o of 0.55% and 0.59% show minimal absorbance signals from the aromatic stretching modes (3000–3100 cm^{-1}) and only low intensity out-of-plane aromatic bands (700–900 cm^{-1}; Fig. 6A). These aromatic bands intensify with increasing rank in coal with R_o of 1.15% and 1.28% (Fig. 6A). The aliphatic stretching region (2800–3000 cm^{-1}) is well developed in all coal samples except anthracite (Fig. 6B). Aliphatic and aromatic stretching bands are only marginally detectable in anthracite (Fig. 6B).

The aromaticity parameter, defined as the intensity ratio of the aromatic stretching bands (3000–3100 cm^{-1}) to the aliphatic stretching bands (2800–3000 cm^{-1}), is presented in Fig. 7 versus R_o (Fig. 7A) and carbon content (Fig. 7B). This parameter is a measure of the proportion of mono-aromatic molecules in the coal structure. For lower rank coals, there is a linear correlation between the rank (expressed either as R_o or carbon content) and the aromaticity parameter, thus indicating progressive aromatisation of coal with increased maturity. For higher rank coal, the structure becomes increas-

Table 1
Vitrinite reflectance, density, ash and ultimate analysis of the coal samples used in this study

Sample	R_o (%)	Density (g/cm^3)	Ash, percentage dry (%)	H, dry ash free	C, dry ash free	N, dry ash free	S, dry ash free	O, dry ash free
Anthracite wc	5.15	1.48	2.6	2.01	95.23	0.91	0.41	1.27
Ammonate wc	1.28	1.47	11.63	5.24	89.85	1.53	0.72	2.659
Bolt wc	1.15	1.46	2.53	5.28	90.92	1.73	0.53	1.53
Herndon wc	0.92	1.44	3.68	5.7	87.29	1.75	0.75	4.51
Elk Run wc	0.88	1.41	2.35	5.45	86.90	1.65	0.65	5.36
FGT6-460 wc	0.59	1.37	9.58	5.77	80.27	1.88	4.34	7.74
FGT6-221 wc	0.55	1.38	16.44	5.71	79.87	1.66	2.88	9.87

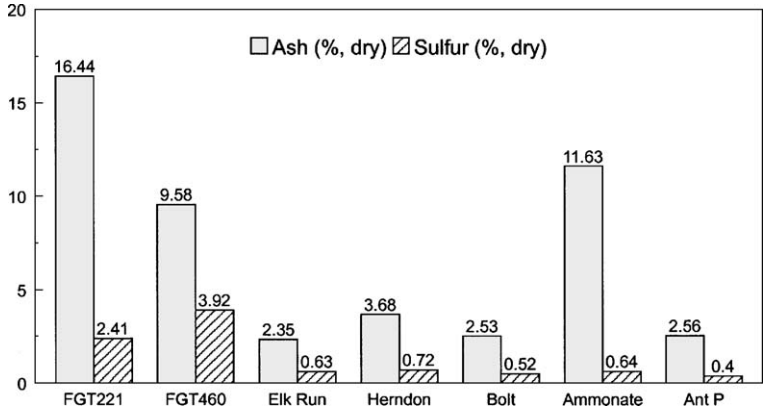

Fig. 2. Ash and sulfur content of the coals (dry basis).

ingly polyaromatic, which explains the decrease of aromaticity parameter in anthracite. The differences in petrographic composition (Fig. 5) are likely to contribute to the scatter in the relationship between the aromaticity parameter and carbon content, as both these parameters are expected to be affected by the maceral composition (Mastalerz and Bustin, 1993).

5. Small angle scattering results

5.1. Pore shape anisotropy and sample orientation

Pore shape anisotropy in coal reflects the magnitude of the principal components of palaeostrain at the time of coalification. In particular, it can be expected that the pore sizes will be reduced in the direction perpendicular to the bedding plane (referred to below as out-of-bedding plane, OBP) compared to in-bedding plane (IBP) directions. As schematically illustrated in Fig. 8 for OBP and IBP samples, the two-dimensional (2D) scattering intensity surfaces are different. For an IBP sample, the pores appear isotropic and the 2D SAS intensity surface is isotropic. The average one-dimensional (1D) scattering curve can then be obtained simply by taking an azimuthal average of the 2D intensity surface. In contrast to this, for an OBP sample, the directional pore anisotropy is reflected in an anisotropic 2D SAS intensity surface. Thus, the section

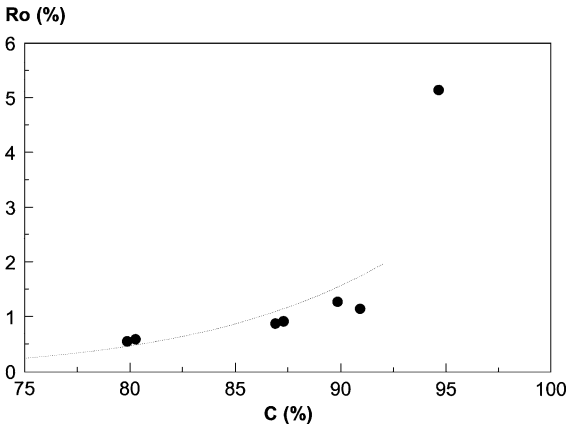

Fig. 3. Relationship between vitrinite reflectance (R_o) and carbon content (dry basis).

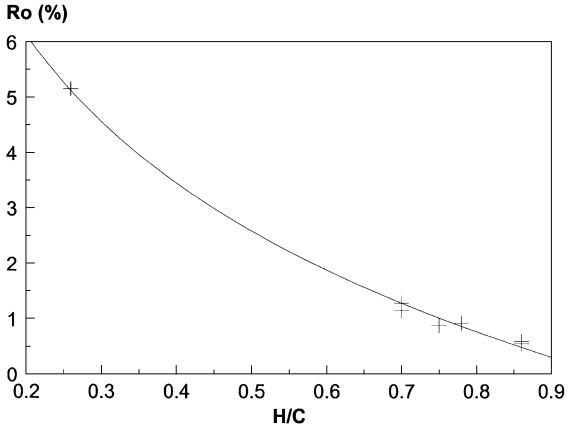

Fig. 4. Relationship between vitrinite reflectance (R_o) and H/C ratio.

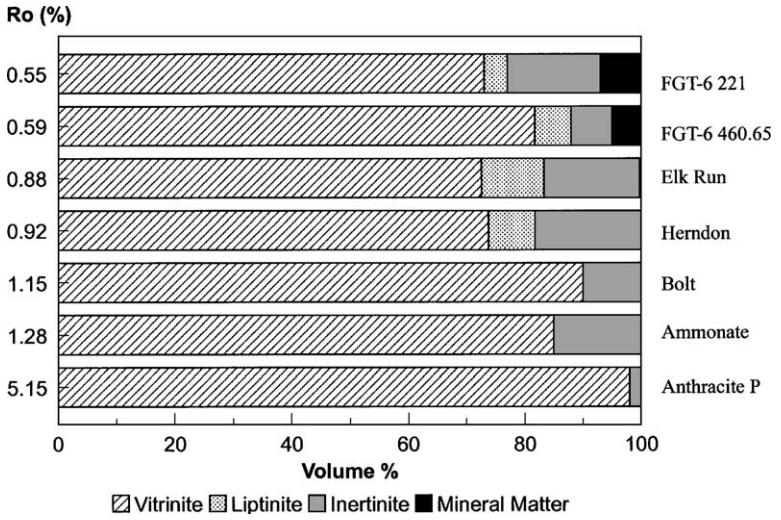

Fig. 5. Maceral composition of the coal samples studied.

average taken along the long (L) and short (S) axes of the footprint of the scattering intensity surface corresponds to the short and long pore axes, respectively. It is expected that the sector average taken along the short axis of the scattering surface would be the same as the radial average of the scattering from the corresponding IBP sample, as in both cases, the scattering originates from the larger pore dimension. These general observations have been confirmed in our previous work on shales (Radlinski et al., 1999).

As discussed in the previous section, SAXS and SANS techniques provide equivalent microstructural information for coals with low ash content. However, the small beam diameter of SAXS instruments (~ 2 mm as opposed to ~ 10 mm for SANS machines) makes them particularly useful for studies on small oriented coal samples. Fig. 9 presents SAXS data for orientation parallel to the bedding plane (IBP), perpendicular to the bedding plane (OBP), and a pellet sample for coal FGT6-460 ($R_o = 0.5\%$). As schematically presented in Fig. 8, the IBP (open circles) and short axis OBP (triangles) scattering curves are very similar, whereas the long axis OBP curve (full squares) is markedly different. The pellet scattering curve (open squares), which represents the average structure of the coal, lies in between the short axis and long axis curves, except in the large-Q region where it shows extra background due to the scattering by resin.

5.2. SAXS results

Small angle X-ray scattering (SAXS) data for seven coals (R_o 0.55% to 3.5%) analyzed in the IBP direction are shown in Fig. 10A. Similar data for corresponding whole coal pellets (except the anthracite) are illustrated in Fig. 10B. It transpires that the shapes for both types of scattering curves for the same coal are very similar, except for the absolute intensity which for a pellet sample is about two times less than for the corresponding solid coal sample. The decrease of scattering intensity for pellet samples in comparison to corresponding solid samples is a simple consequence of the (theoretical) volume average coal density for pellets being approximately 50% less than for corresponding solid coals, the remaining 50% of the volume being occupied by resin. Resin only contributes to a Q-independent, small scattering background of the order of 0.1 cm^{-1}.

Based on our SAXS data, there is a general trend for coal anisotropy to decrease with maturity, which results in the IBP and pellet scattering becoming more and more similar as coal rank increases. This is illustrated in Fig. 10C for three selected coal samples

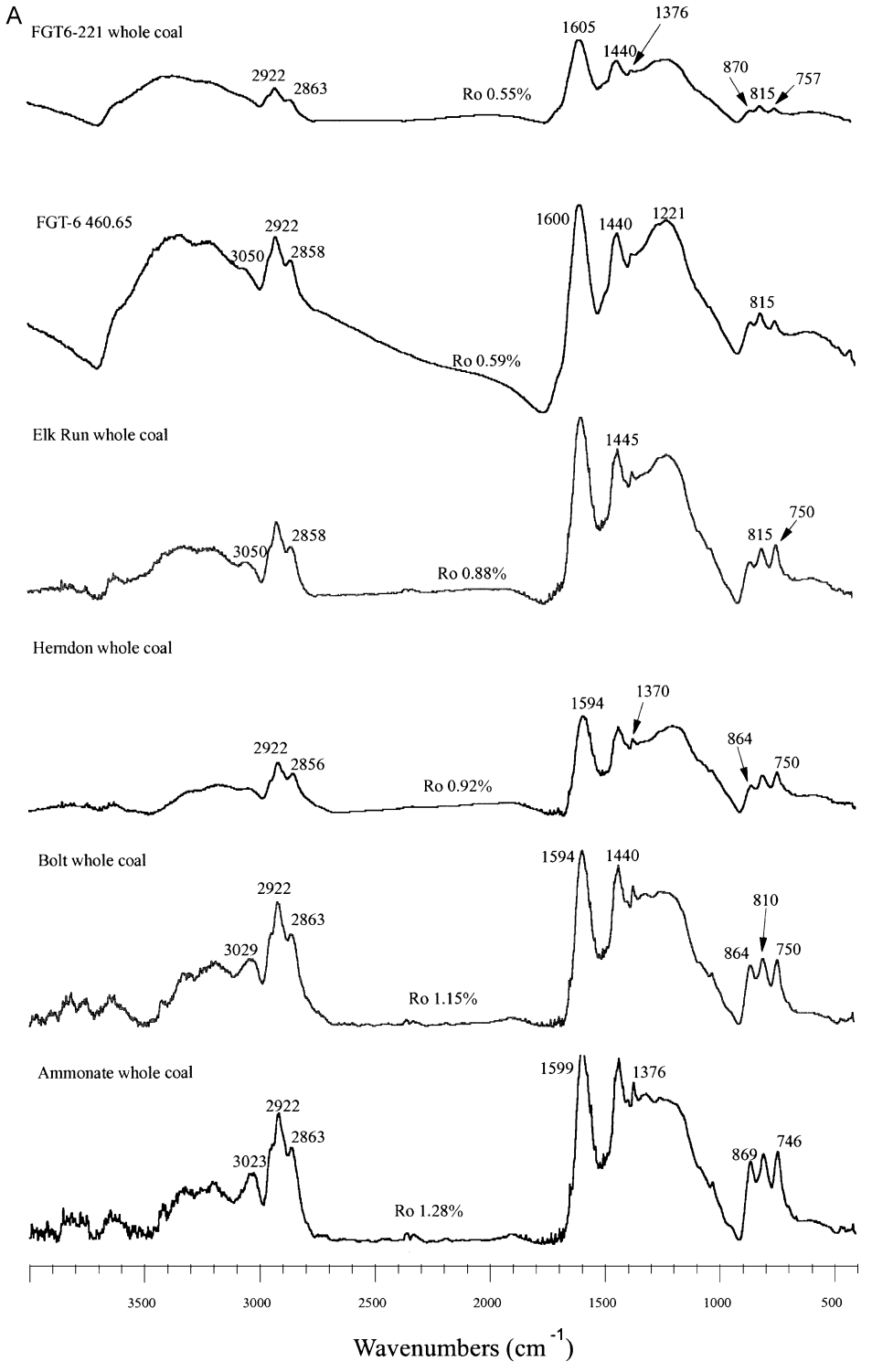
A
FGT6-221 whole coal
2922
2863
Ro 0.55%
1605
1440
1376
870
815
757
FGT-6 460.65
3050
2922
2858
Ro 0.59%
1600
1440
1221
815
Elk Run whole coal
3050
2858
Ro 0.88%
1445
815
750
Herndon whole coal
2922
2856
Ro 0.92%
1594
1370
864
750
Bolt whole coal
3029
2922
2863
Ro 1.15%
1594
1440
810
864
750
Ammonate whole coal
3023
2922
2863
Ro 1.28%
1599
1376
869
746
3500
3000
2500
2000
1500
1000
500
Wavenumbers (cm -1)

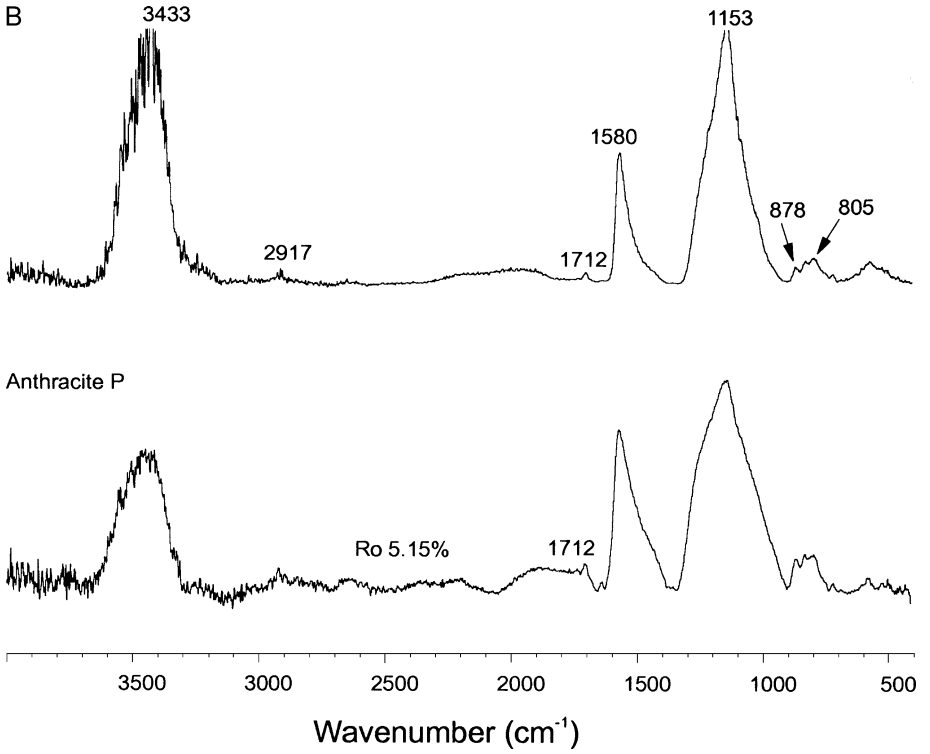

Fig. 6. (A) FTIR spectra of coal samples with vitrinite reflectance from 0.55% to 1.28%. Spectra were obtained on kerogen concentrates (after removal of mineral matter from coal). (B) FTIR spectra of anthracite ($R_o = 5.15\%$). Spectra were obtained on kerogen concentrates (after removal of mineral matter from coal).

of different rank, with pellet data multiplied by a factor close to 2 and selected to bring the scattering intensity of a pellet to the level of the scattering intensity by the corresponding solid coal. Our data show very clearly that the small angle X-ray scattering curves obtained for crushed pellets are very close to those obtained for solid coal samples cut out parallel to bedding, especially for coals of high rank.

5.3. SANS and USANS results

Small angle neutron scattering (SANS and USANS) data for 12 samples prepared from six coal beds of different rank (coal of IBP orientation and coal pellet) are shown in Fig. 11. Fig. 11A and C shows the combined SANS and USANS scattering data for coal of IBP orientation and coal pellets, respectively, whereas Fig. 11B and D focus on the SANS data in the Q-range similar to that covered by SAXS data (Fig. 10).

In the small-Q region (10^{-5} Å$^{-1} < Q < 10^{-2}$ Å^{-1}), the scattering data for coal pellets and coal samples of IBP orientation look similar (Fig. 11A,C). For all the samples for which the USANS data are available, the scattering intensity can be represented on the log–log scale by a straight line with a slope close to -3, which indicates a very rough surface fractal pore–matrix interface (Radlinski et al., 1996). In this region, the scattering intensity is dominated by pores of linear dimensions in the range 25 μm $< 2.5/Q <$ 250 Å. In the large-Q region (0.01 Å$^{-1} < Q <$ 0.25 Å^{-1}; pore size range, 10 to 250 Å), the shape and intensity of the scattering curve clearly depends on the sample type and rank. Although the overall trend is similar to that observed with SAXS (Fig. 10; scattering intensity generally decreasing with coal rank, marked scattering intensity increase for the two FGT6 coals), there are specific differences between sample types that reflect the microstructural effects of the degree

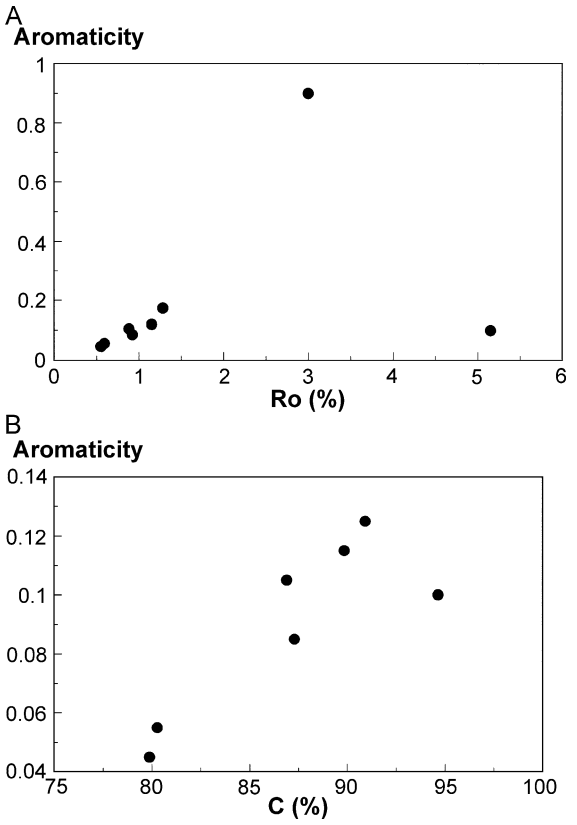

Fig. 7. (A) Relationship between vitrinite reflectance (R_o) and aromaticity parameter as calculated from FTIR analysis. (B) Relationship between carbon content and aromaticity parameter as calculated from FTIR analysis.

of anisotropy, inorganic component and the maceral composition.

In the Q-region 10^{-3} Å$^{-1} < Q < 3 \times 10^{-3}$ Å^{-1}, for some samples, there is a notable gap between the USANS and SANS data. This gap can only be eliminated at the cost of substantially longer acquisition times for USANS data, which was not available in some cases. The lack of overlap between SANS and USANS data creates a small uncertainty when joining the two curves. In our previous publication (Radlinski et al., 2001), a sensitivity analysis was undertaken to determine the consequent uncertainty in the computed pore size distribution and specific surface area. It was concluded that the relative error for the *absolute* value of pore density is pore-size independent and typically no larger than $+/-50\%$, whereas the specific surface area for molecular size probes is extrapolated from data with relative error no larger than $+/-10\%$.

A common feature of both sets of data (both SAXS and SANS/USANS) is a flattening of scattering curves for Q values larger than approximately 0.05 Å^{-1} (Fig. 11A and C). In the following analysis of the pore size distribution and specific surface area, we have discarded the part of the spectra in this region. This is equivalent to discarding part of the mathematically obtained information pertaining to pores smaller than $2.5/Q = 50$ Å (Radlinski et al., 2000a,b). This part is likely to be affected by background scattering which, for the purpose of further data analysis, was estimated and subtracted. This was done by choosing a background value that puts the data points approximately on a straight line on the log–log scale in the large-Q region. We believe that the flattening is due to a structural inhomogeneity of the size of about 25 Å that is possibly lamellar in nature. Therefore, we used 25 Å as the lower size limit of the pore space that can be reasonably analyzed using the spherical pore approximation. Significantly, the 25 Å inhomogeneity is much more pronounced in the SAXS data (Fig. 10) than SANS data (Fig. 11).

6. Pore size distribution

The pore size distribution (also known as pore number density) is defined as the number of pores within the narrow size (diameter) interval between r and $r+dr$, $N(r,r+dr)$, divided by the total number of pores (of diameter between 25 Å to 20 μm in this work), N: $f(r) = N(r,r+dr)/N$. In simple terms, $f(r)$ is the proportion of pores of diameter within a narrow band centered on r within the total population of pores. The pore size distribution, $f(r)$, was computed from SANS/USANS data for each sample using the standard Spherical Pore Approximation procedure (Appendix A; Radlinski et al., 2001; Hinde, in press) and expressed as a histogram on a logarithmic r-scale. Scattering length densities used are listed in Table 2. Although similar calculations could technically be performed for SAXS data, this was not done owing to the complications in the interpretation of SAXS results caused by high ash content of some coal (Table 1). By the nature of the small angle

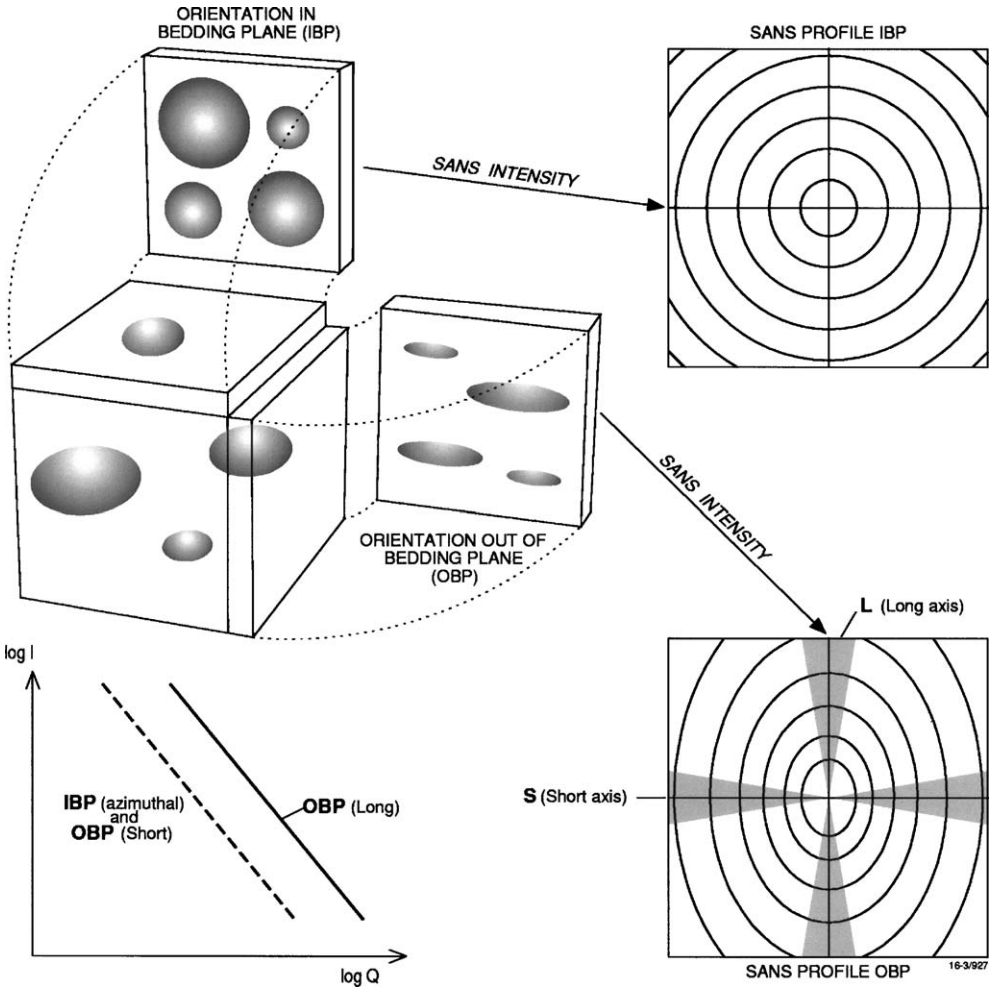

Fig. 8. From upper left corner, clockwise: (1) Schematic graphical representation of the shape of pores as present in coal slices cut out in-the-bedding plane (IBP) and perpendicular to the bedding plane (described as out-of-bedding plane, OBP). During the SANS experiment, the neutron beam is incident on a sample perpendicular to the large face, and a planar 2D detector comprising a large number of elements (pixels) is placed at some distance behind the sample. (2) Schematic SANS intensity profile observed with a 2D detector for an IBP oriented coal sample. The concentric circles are isointensity lines, with intensity increasing towards the center of the detector. The scattering pattern has an axial symmetry, which reflects the fact that pores are statistically identical in any in-plane direction (i.e., isotropic). One-dimensional SANS curves are obtained from such isotropic scattering patterns by taking an azimuthal average over the entire detector area. The scattering vector, Q, is proportional to the distance between a detector element (pixel) and the detector center. (3) Schematic SANS intensity profile observed with a 2D detector for an OBP-oriented coal sample. The isointensity lines are now ellipsoidal, reflecting the fact that statistically the pores are larger in the in-bedding plane directions than in the perpendicular-to-the-bedding direction. Shaded sectors indicate those sections of the detector over which the signal has been averaged to produce the in-bedding plane (along the short axis of the ellipsoid) and out-of-bedding (along the long axis of the ellipsoid) one-dimensional SANS curves. The sectors are selected to be narrow enough (typically no more than 20°) to well approximate isointensity lines with circular arcs. (4) One-dimensional SANS data averaged as described in (2) and (3) and plotted on a log–log scale, where Q is the scattering vector (proportional to the scattering angle), and I is the scattering intensity. The azimuthal average for the in-bedding plane sample (IBP) and the sector average for the perpendicular-to-bedding sample along the short axis of the 2D SANS ellipsoid (OBP short) are expected to fully coincide, as they both represent scattering on the in-bedding plane elements of the pore space. The sector average for the perpendicular-to-bedding sample along the long axis of the SANS ellipsoid (OBP long) corresponds to scattering on the gravitationally squashed, perpendicular to the bedding plane, elements of the pore space, and for anisotropic coals it is distinctly different from the other two averages.

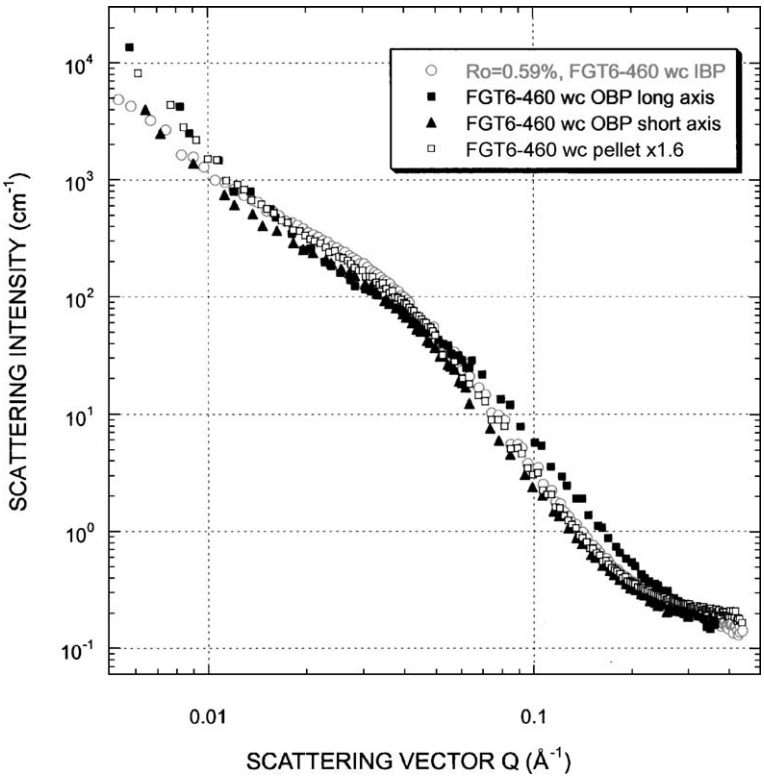

Fig. 9. SAXS data for coal FGT6-460 ($R_o = 0.59\%$) in direction parallel to bedding (IBP), perpendicular to bedding (OBP) and for coal pellet. Scattering cross section values for the pellet are multiplied by 2, to compensate for the presence of mounting medium, as discussed later in the text.

scattering method, the calculated pore size distribution includes all pores, whether they are accessible via pore throats or not. A description of methodology and numerical details can be found elsewhere (Radlinski et al., 2001; Hinde, in press). The specific formulae used in calculations are also listed in the Appendix A.

Pore size distributions obtained for coal samples oriented parallel to bedding and for coal pellets are illustrated in Fig. 12A and B. The analysis of combined SANS/USANS data provides quantitative pore size distributions in the pore size range 10 Å to about 15 μm (1 μm = 10,000 Å), whereas the range of pore sizes which can be determined from SANS data alone is 10 to 1000 Å. In every case, the pore size distribution is very broad and includes contribution from every pore size within the entire range.

It is apparent that, with the exception of the small pore size region for some low rank coals, the pore size distributions follow the power law $f(r) = Ar^B$, where the exponent B is close to 4 (Fig. 12A and B). This is a direct consequence of the power law (surface fractal-like) scattering intensity (Fig. 11) because the fractal pore–matrix interface is equivalent to a polydisperse system of pores with the number distribution of pore sizes (i.e., the number of pores with radii between r and $r + dr$) given by $f(r)dr = f_{00} \times r^{-(1+D)}dr$ (Schmidt, 1982; Pfeifer and Avnir, 1983). In this formula, f_{00} is a constant and D is the fractal dimension determined from the (negative) slope of the power–law scattering: $D = \text{slope} + 6$.

Numerical values of parameters A and B determined from the least squares fits to distributions presented in Fig. 12 are listed in Table 3. Although in some cases, it is convenient to use such a simple

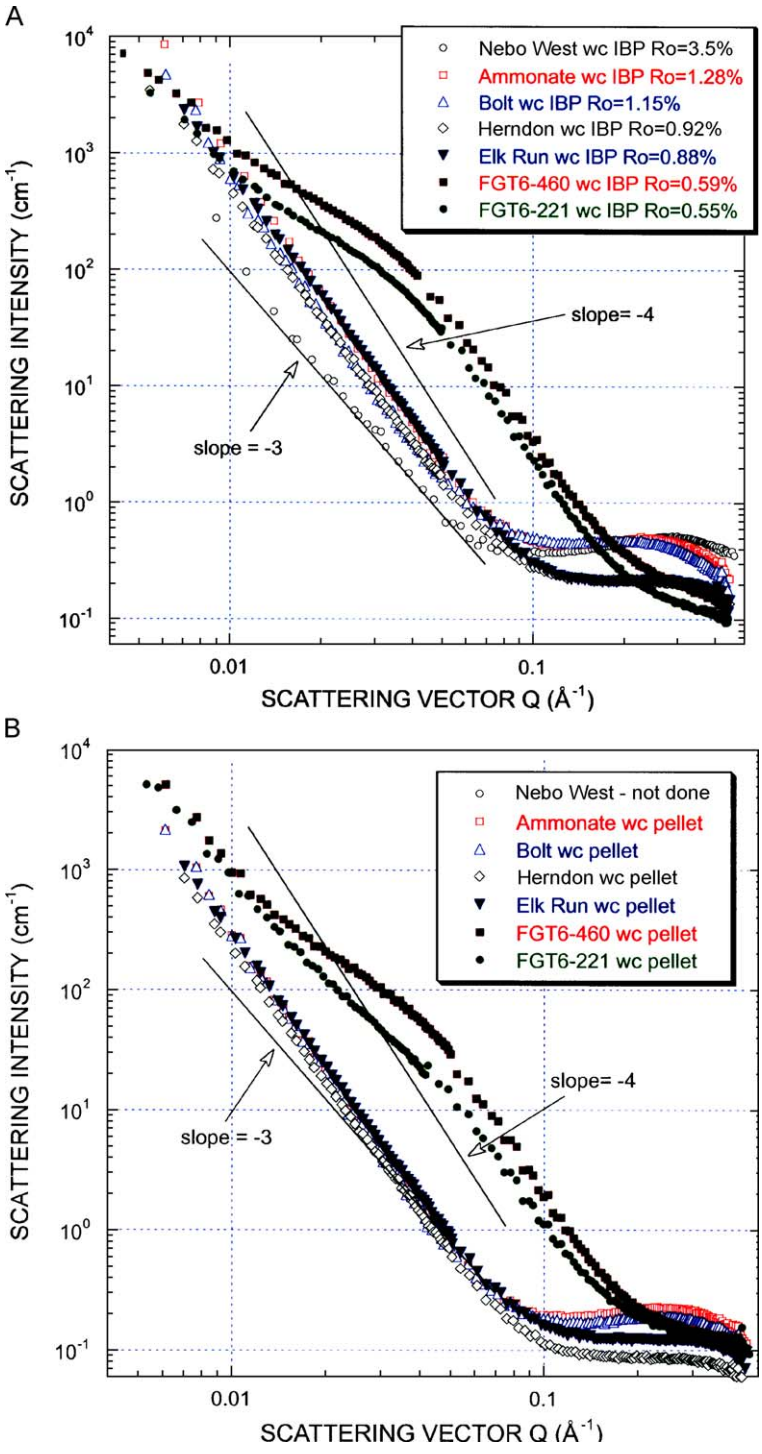

Fig. 10. (A) SAXS data for coal samples oriented parallel to bedding (IBP). Nebo West coal ($R_o = 3.5\%$) from Australia is added to have wider representation of coal rank. (B) SAXS data for pellet samples of coals of different rank. (C) Comparison of SAXS data for coal samples oriented parallel to bedding and the same coals mounted in pellets.

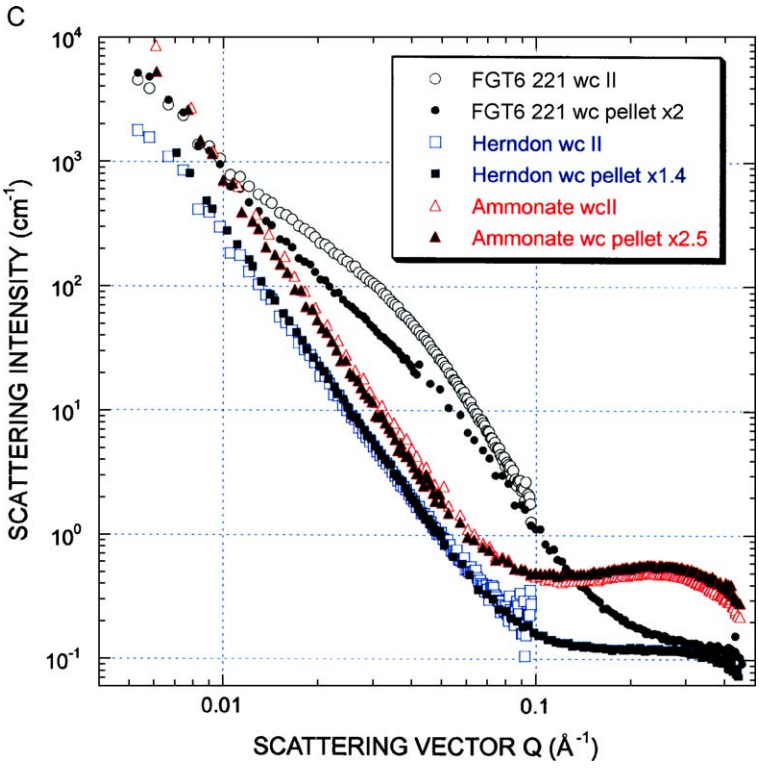

Fig. 10 (*continued*).

two-parameter representation of the pore size distribution, it should be stressed that our computations (Fig. 12) are quite general and are not limited to the fractal model.

7. Evolution of the mesopore and macropore size distribution with rank

The shape of a SANS curve depends on the pore size distribution and the pore content. This simply follows from the scattering intensity being dependent on (1) the size and number of the scattering objects (pores in this case), and (2) scattering contrast between the coal matrix and the matter contained within the pores. A convenient way of depicting the evolution of the pore space with rank is to plot the pore number density (equivalent to the pore size distribution), $f(r)$, versus rank for several selected pore sizes, r, and compare the result with a similar plot of the scattering intensity versus rank for Q-values corresponding to these pore sizes, $Q = 2.5/r$. Figs. 13 and 14 show the evolution of the scattering intensity and pore number density with rank expressed by vitrinite reflectance in oriented coal samples and coal pellets for several pore sizes increasing by a factor of 10 from 10 to 100,000 Å (10 μm).

Firstly, the scatter of SANS intensity experimental points for oriented coal samples (Fig. 13A) is not much different from the scatter of the pellet data (Fig. 13B). This indicates that pellets have been prepared in a consistent way with a uniform coal grain volume filling factor. Secondly, for samples oriented parallel to bedding, there is an apparent contraction of the pores with rank on small scales (10 to 1000 Å) and a simultaneous expansion on larger scales (1 to 10 μm; Fig. 14A). This result is an artefact which reflects the evolution of the anisotropy of coal with rank and underlines the importance of scattering data obtained from pellet samples. The corresponding pore size distribution data for pellets, which is averaged over all the possible orientations, indicate a systematic

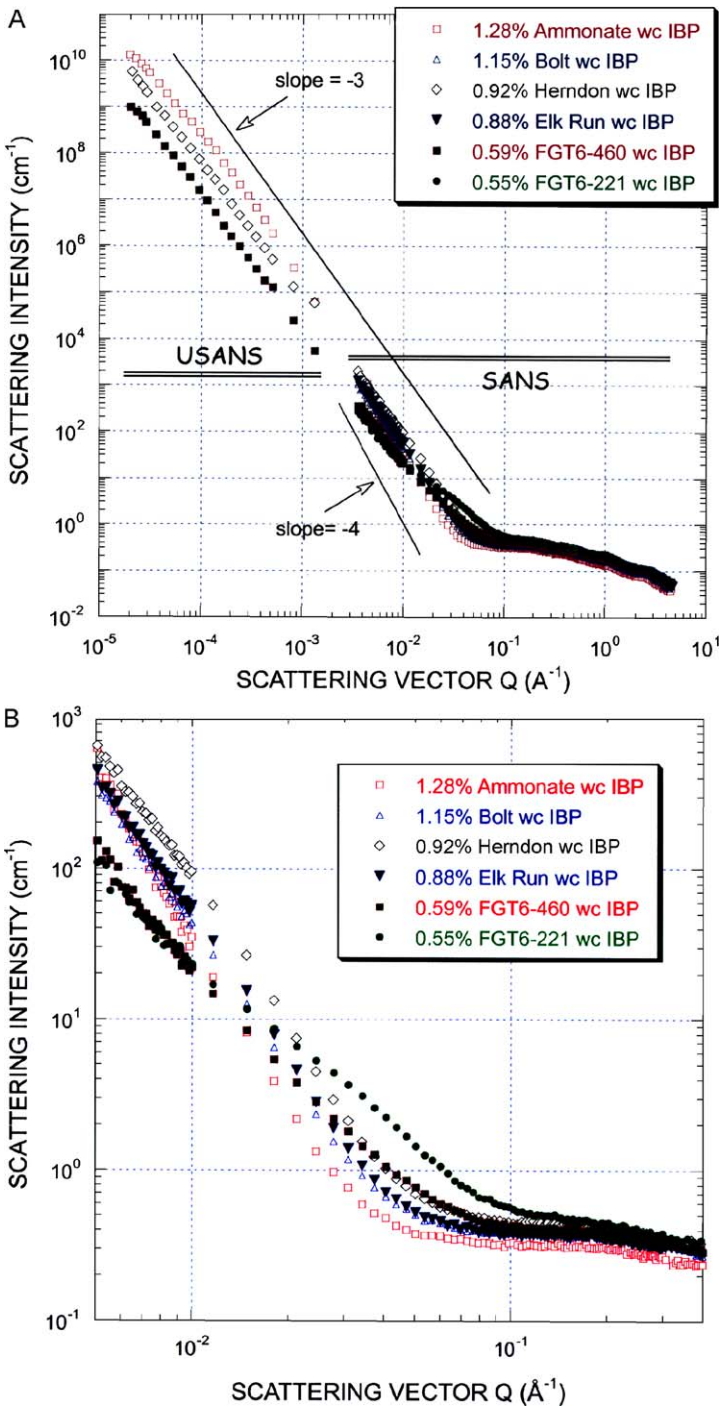

Fig. 11. (A) SANS and USANS data for coal samples of different rank oriented parallel to bedding. (B) Part of data from (A) within the scattering vector range of 4×10^{-1} to 5×10^{-3} Å^{-1}. (C) SANS and USANS data for coal pellets of different rank. (D) Part of data from (C) within the scattering vector range of 4×10^{-1} to 5×10^{-3} Å^{-1}.

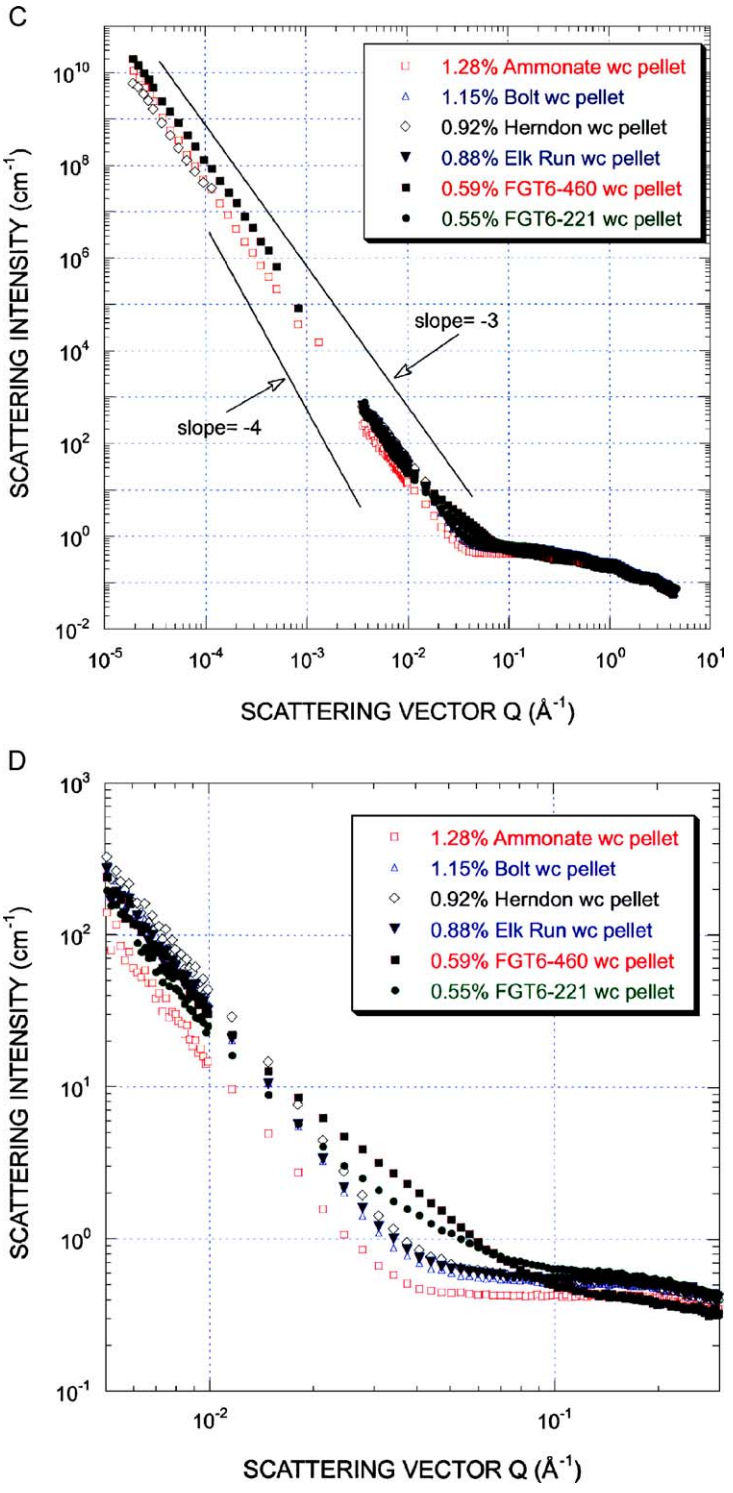

Fig. 11 (*continued*).

Table 2
Scattering length density for the coal samples calculated from their elemental composition and specific density of these coals

Sample	Ammonate	Bolt	Herndon	Elk Run	FGT6-460	FGT6-221
SLD neutrons ($\times 10^{10}$ cm^{-2})	2.86	3.16	2.88	3.10	2.51	2.46
SLD X-rays ($\times 10^{11}$ cm^{-2})	1.31	1.30	1.29	1.26	1.23	1.24
R_o (%)	1.28	1.15	0.92	0.88	0.59	0.55

Elemental composition of organic components is given in Table 1. For ash, the average composition, 49% SiO_2 + 25% Al_2O_3 + 13% Fe_2O_3 + minor minerals, and density 2.4 g/cm^3, gives the SLD for neutrons equal to 3.6×10^{10} cm^{-2} and SLD for X-rays equal to 2.4×10^{11} cm^{-2}.

decrease of the pore number density with rank for all pore sizes, except perhaps for the largest pores (Fig. 14B). The scatter of data points is significant, especially for the smaller pore sizes.

The SANS intensity data indicate a systematic evolution of the pore space with rank on all scales (Fig. 13A and B). The intensity data for pellet samples exhibit a decrease of scattering intensity with rank for all pore sizes (Fig. 13B). This decrease of intensity seems to parallel the decrease in pore number density observed for the same pore sizes, perhaps with the exception of the 100 Å pores for which the pore number density seems to be pore-size-independent (Fig. 14B—note that symbols corresponding to various pore sizes are the same in Figs. 13 and 14). This may indicate that the smallest pores are being increasingly clogged with thermally generated bitumen with increased rank, as first suggested by Janowsky (1984) and recently demonstrated using SANS by Boreham et al. (2003).

8. Specific surface area

For porous systems with the pore size distribution covering multiple length scales, the specific internal surface area, SSA, depends on the size of the measuring probe. In this work, the SSA, as a function of probe size r, was calculated from the pore size distribution histograms using Eq. (8.1) in the Appendix A. Fig. 15 shows the calculated specific surface areas versus the probe size and the extrapolation to a molecular probe size of 4 Å. It should be noted that the procedure for estimating the specific surface area for probe sizes of the order of several Å, typical for nitrogen, methane and carbon dioxide molecules, was to extrapolate the SANS-derived data in the region 20 Å $< r <$ 100 Å, rather than rely on the noisy result directly calculated for the smallest probe sizes (Fig. 15). As the extrapolation procedure is only based on a few experimental points for probe sizes smaller than about 100 Å, the uncertainty is significant, generally of the order of +/− 50% of the quoted value.

An independent measurement of the specific surface area was done using the nitrogen adsorption method (probe size: 4 Å). The nitrogen adsorption results are given in Table 4 and also shown in Fig. 16, where they can be compared with SANS-derived values for surface area obtained by extrapolation to $r = 4$ Å. For this comparison, we also included results obtained for vitrinite. Comparison should be made between the N_2 and SANS pellet data because the SANS IBP data do not properly average over the 3D microstructural anisotropy of the coal matrix. It is evident that both sets of data follow the same pattern versus R_o, with N_2 values being systematically lower, by a factor of about 2–6, than the neutron values. Given that: (1) the nitrogen method only accounts for the accessible (open) pores whereas SANS is sensitive to both open and closed pores, (2) the degree of nitrogen saturation may be sample-specific and cannot be controlled and (3) the presence of residual moisture in SANS samples can increase the calculated SSA by a factor of up to 1.44 (for full water saturation of the smallest pores), the agreement between the two methods is good.

9. Total porosity

The pore space in coals comprises three distinct systems: micropores (size: less than 50 Å), mesopores (size: 50 to 500 Å) and macropores (size: 500 Å to about 50 μm) (Littke and Leythaeuser, 1993). Traditionally, the micropores have been studied by measuring heats of wetting in different liquids, whereas mesopores and macropores with mercury injection porosimetry.

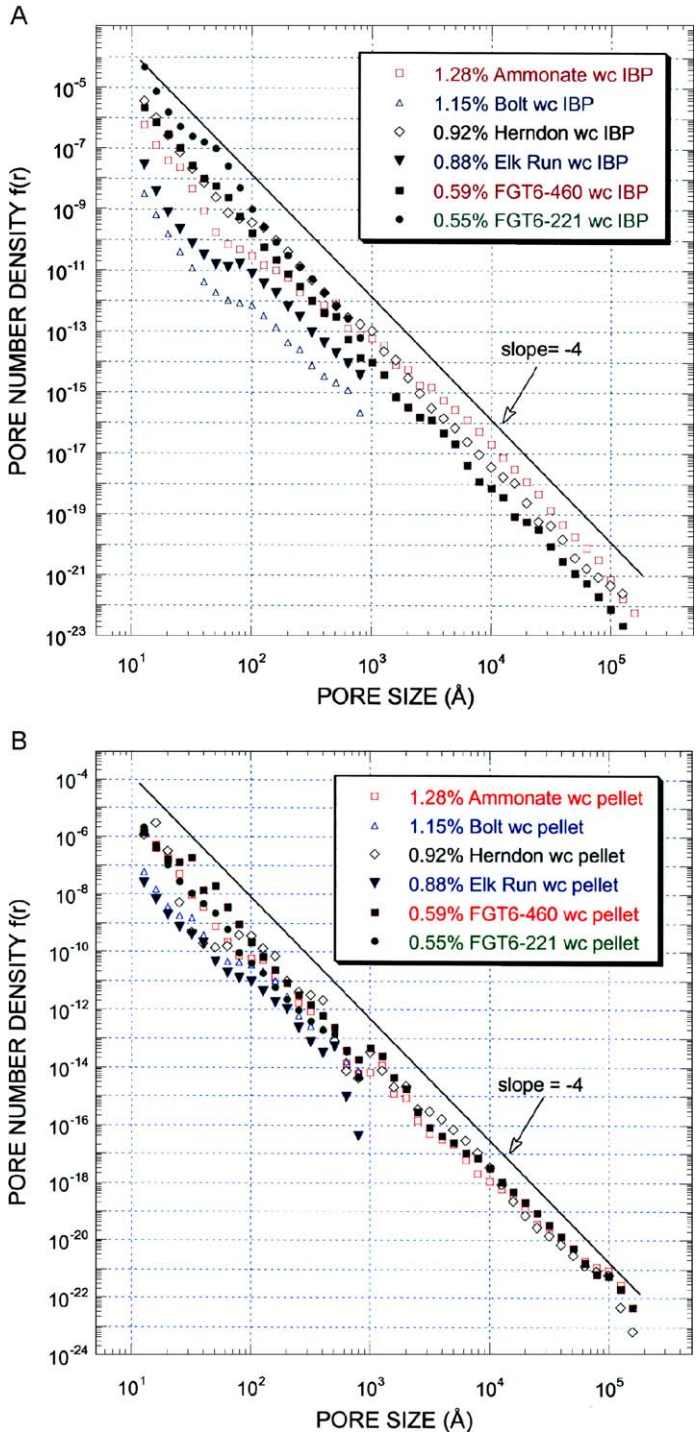

Fig. 12. (A) Pore size distribution calculated from SANS and USANS data for coal samples oriented parallel to bedding (IBP). (B) Pore size distribution calculated from SANS and USANS data for coal pellets.

Table 3
Values of parameters A and B obtained by Fig. 12 to the power law model $f(r)=Ar^B$

Sample		A	B	Correlation coefficient R
Ammonate wc	IBP	1.09×10^{-3}	−3.53	0.97
	Pellet	5.14×10^{-3}	−3.88	0.999
Bolt wc	IBP	not done		
	Pellet	not done		
Herndon wc	IBP	3.82×10^{-2}	−3.99	0.99
	Pellet	6.46×10^{-3}	−3.89	0.68
Elk Run wc	IBP	not done		
	Pellet	not done		
FGT6-460 wc	IBP	4.98×10^{-2}	−4.194	0.999
	Pellet	2.80×10^{-2}	−4.01	0.99
FGT6-221 wc	IBP	5.063×10^{-2}	−4.791	0.98
	Pellet	8.29×10^{-2}	−4.53	0.99

The SAS method provides access to micropores, mesopores and macropores (up to about 20 μm diameter) in one experiment. This is well illustrated by SAXS data presented in Fig. 10A. For Q-values smaller than about 0.1 $Å^{-1}$, corresponding to pore sizes larger than about $2\pi/Q=65$ Å, an increase in the scattering intensity due to the onset of the fractal (mesopore and macropore) system is observed. This intensity increase is mirrored in SANS/USANS data (Fig. 11) indicating a fractal system of mesopores and macropores which has been modeled by a system of polydisperse spheres, leading to the specific surface areas and pore size distributions discussed above (Figs. 12 and 15). Thus, the distributions and values presented in Figs. 12 and 15 pertain exclusively to the mesopore and macropore system.

The total porosity for each sample can be determined by summing the volumes of all pores in the pore size distribution. The result is presented in Fig. 17, superimposed on the published coal porosity trend curves (Berkowitz, 1979). It is apparent that small angle, scattering-derived total macroporosity values are consistent with the established trend throughout the entire coal rank range, thus indicating only a minor contribution from micropores.

In the large-Q region of SAXS data (Q larger than 0.1 $Å^{-1}$), a broad scattering peak centered at about $Q_{ave}=0.25$ $Å^{-1}$ is present (Fig. 10A). The intensity of this peak increases with increasing coal rank. The presence of the peak suggests a microstructure comprising lamellae of polyaromatic hydrocarbon sheets spaced at an average distance of $D=2\pi/Q_{ave}=25$ Å. Although numerical modeling of scattering by two-phase lamellar systems is possible, in this particular case, the SANS data (Fig. 11A) show very low intensity of the polyaromatic peak compared to corresponding SAXS data (Fig. 10A). This combination of a strong SAXS and weak SANS signature, when analyzed using the numerical SAXS and SANS scattering length density data for the organic and inorganic components of coal (Radlinski and Hinde, 2001), strongly suggests that the scattering contrast in the micropore region is *predominantly not* between the polyaromatic sheets of coal matrix and void, or generated bitumen, or water. These scenarios would result in strong SAXS and SANS signature for matrix–void scattering, weak SAXS and SANS signature for matrix–bitumen scattering and weak SAXS and strong SANS signature for matrix–water scattering. The most likely conclusion, consistent with the strong SAXS signature and weak SANS signature, is that the scattering occurs predominantly between the polyaromatic sheets and intercalated inorganic matter. In other words, the micropores appear to be significantly clogged with nearly molecular-size particles of inorganic matter, probably clays.

This conclusion, based on SAXS and SANS contrast considerations, is strongly supported by nitrogen adsorption data which confirm that there is no micropore contribution to the specific surface area, even for high-rank coal (Fig. 16). Based on the well-known trends, such a contribution is expected to be of the order of 100–200 m^2/g for coals with carbon content above about 85% (Berkowitz, 1979), compared to the measured values of the order of 1 m^2/g in this region (Fig. 15). Based on geometrical considerations, the maximum possible micropore contribution to coal porosity (assuming polyaromatic sheet spacing 25 Å throughout the entire sample volume) is 570 m^2/g.

The clogging of lamellar micropores with inorganic matter does not preclude the possibility that other types of micropores, mesopores and macropores may be available for fluid transport. We note that the loss of microporosity at the end of "oil

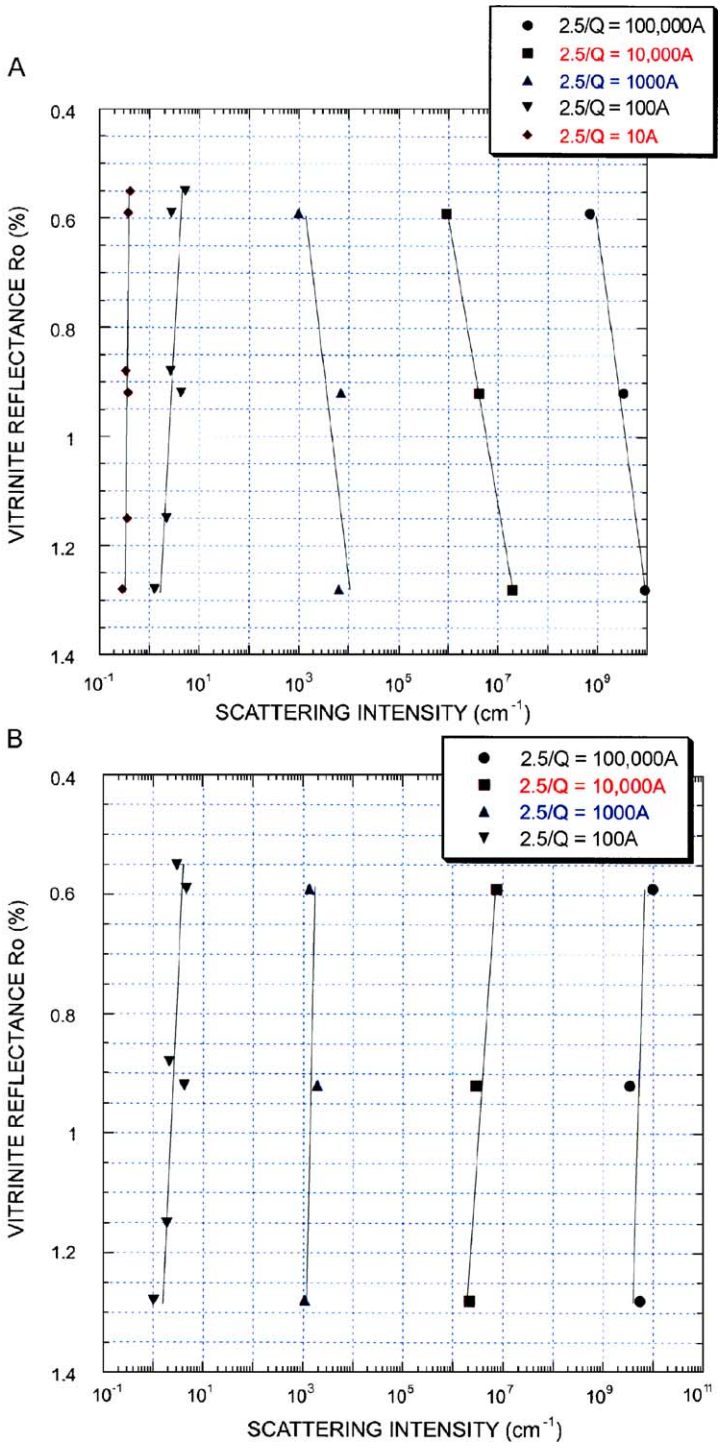

Fig. 13. (A) Scattering intensity versus vitrinite reflectance for selected pore sizes in coal samples oriented parallel to bedding (IBP). (B) Scattering intensity versus vitrinite reflectance for selected pore sizes in coal pellets.

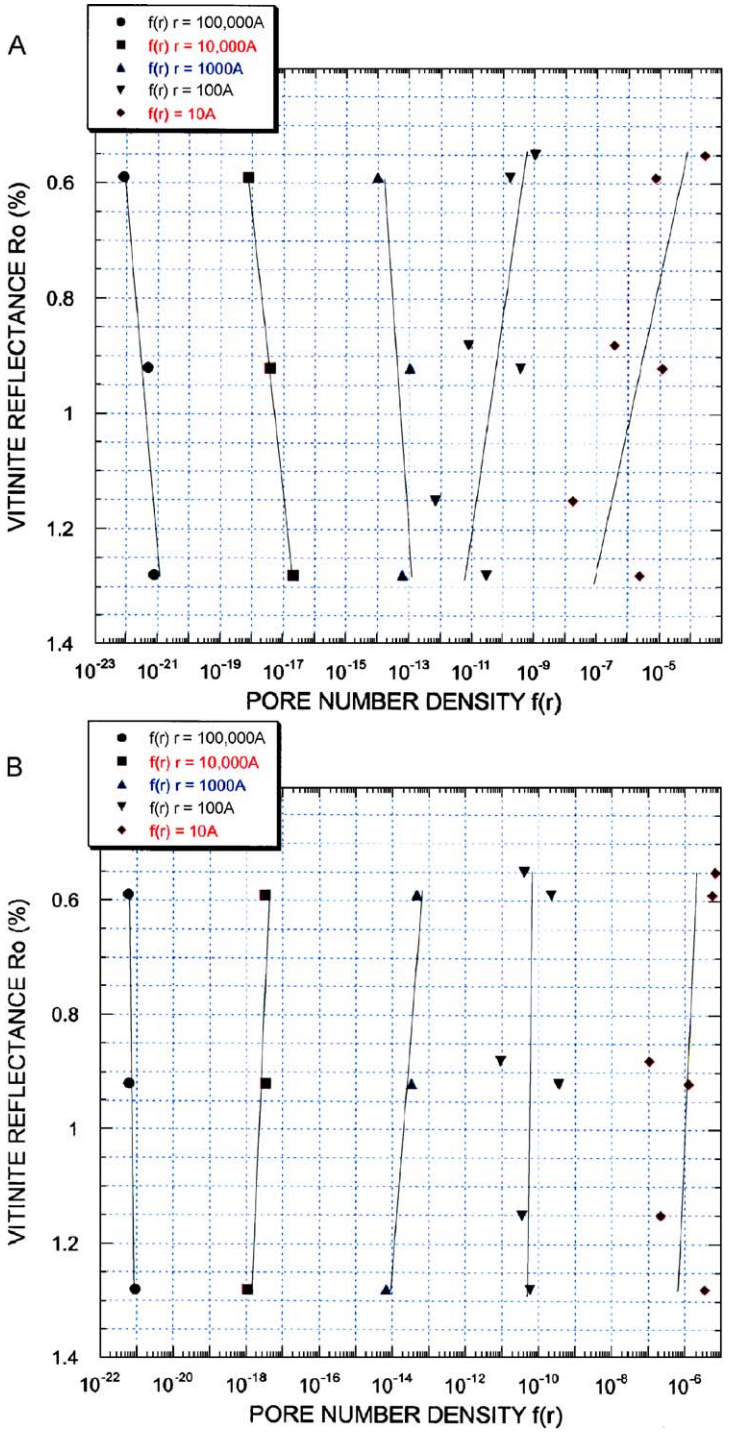

Fig. 14. (A) Pore number density versus vitrinite reflectance for selected pore sizes in coal samples oriented parallel to bedding (IBP). (B) Pore number density versus vitrinite reflectance for selected pore sizes in coal pellets.

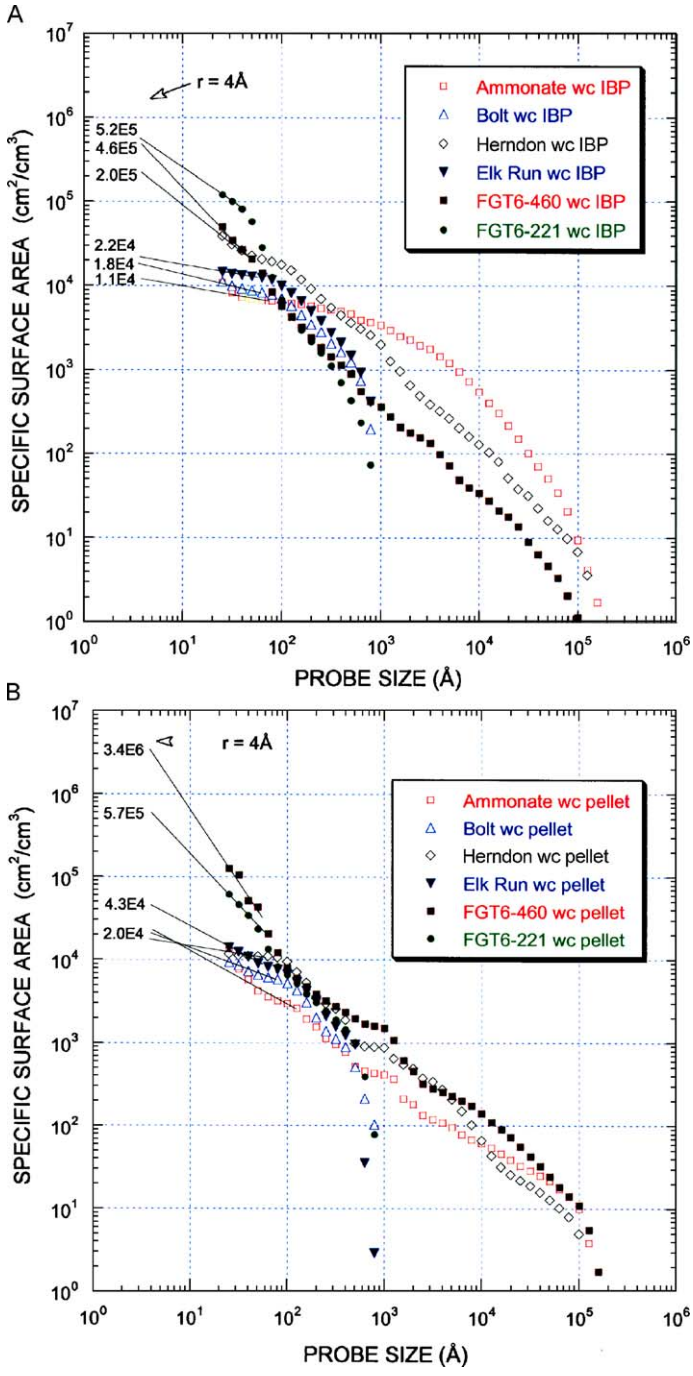

Fig. 15. (A) Specific surface area versus probe size for coal samples oriented parallel to bedding (IBP). (B) Specific surface area versus probe size for coal pellets.

Table 4
Experimental specific surface areas ($\times 10^3$ cm^2/cm^3) at a probe size of 4 Å, obtained from N_2 adsorption and from the extrapolation of SANS data, for six whole coal pellet samples

Method	Ammonate	Bolt	Herndon	Elk Run	FGT6-460	FGT6-221
	R_o: 0.92%	R_o: 0.15%	R_o: 0.92%	R_o: 0.88%	R_o: 0.59%	R_o: 0.55%
Single point	ND	5.26	4.90	4.65	361	242
BET	ND	5.40	4.90	4.79	376	252
Langmuir	ND	7.45	6.77	6.77	522	348
SANS extrapolated to 4 Å	22	21	20	43	3400	570

The nitrogen adsorption data were converted from cm^2/g to cm^2/cm^3 units using the nominal density of solid coal matrix (Table 1).

generation window" (at R_o value of about 1%) has been observed by Janowsky (1984) and tentatively explained by trapping generated bitumen within the micropores, an interpretation supported by the finding of Harris and Petersen (1979) that solvent extraction creates new micropores in coal. Boreham et al. (2003) have recently demonstrated a progressive saturation of mesopores with bitumen and rearrangement of mesopore architecture within the "hydrocarbon generation window".

10. Conclusions

This study demonstrates that SANS/USANS and SAXS techniques are valuable in obtaining the pore

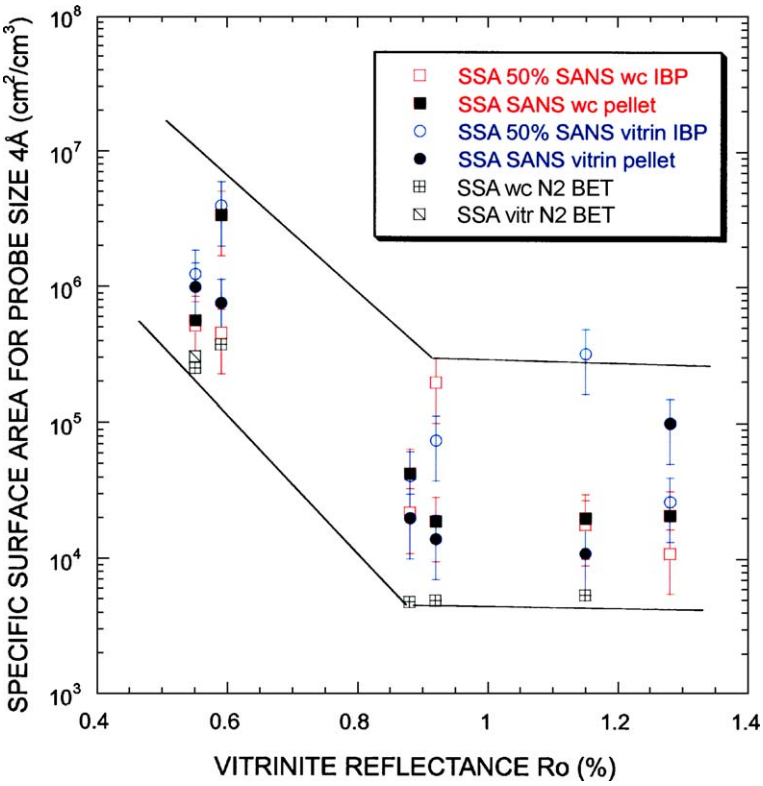

Fig. 16. Comparison between specific surface area (cm^2/cm^3) for coals of different ranks extrapolated to probe diameter 4 Å from SANS and nitrogen adsorption techniques.

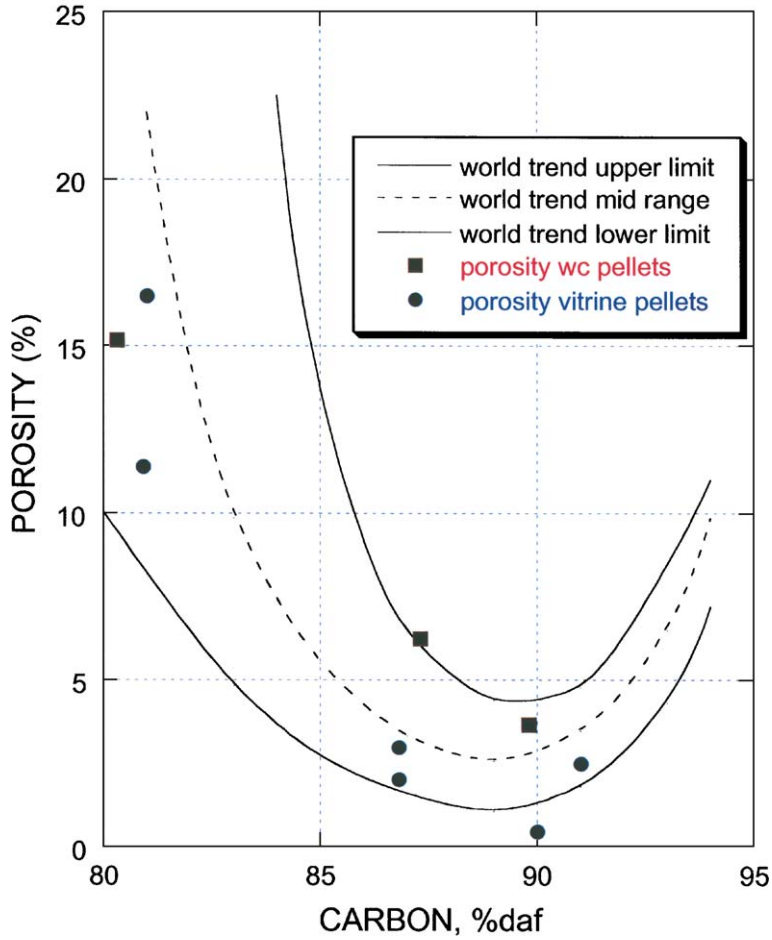

Fig. 17. Porosity of coals and vitrinites of various rank calculated from SANS/USANS data for pellets. Pore size range: 25 Å to 10 μm.

size distribution and specific surface area of a representative coal sample by using crushed coal pellets. SANS and USANS are sufficient to quantify these parameters for a very wide range of pore sizes. SANS/USANS and SAXS data for whole coal pellets compare very well to those obtained for whole coal samples oriented parallel to bedding.

Surface area determined by a nitrogen probe is somewhat lower than that derived from SANS/USANS data. This is due to the possible presence of moisture in SANS samples, and to the fact that the SANS/USANS technique measures all the pores whereas the nitrogen adsorption method probes only the open (accessible) pores. The numerical values obtained by the scattering and nitrogen adsorption methods show remarkably similar trends versus vitrinite reflectance.

Acknowledgements

Marc Bustin of the University of British Columbia is thanked for measurements of surface areas using the nitrogen adsorption method. The authors are indebted to D.G. Wozniak for his expert assistance with the SANS measurements. J. Pashin and J.R. Levine are thanked for their valuable comments and suggestions. The research at Oak Ridge was sponsored in part by the U.S. Department of Energy under Contract No. DE-AC05-00OR22725

with the Oak Ridge National Laboratory, managed by the UT-Battelle, LLC. This work benefited from the use of IPNS, which is funded by the Division of Materials Science, Office of Basic Energy Sciences, U.S. Department of Energy, under Contract W-31-109-ENG-38 to the University of Chicago. A.P. Radlinski and A.L. Hinde publish with the permission of the Chief Executive Officer, Geoscience Australia.

Appendix A

Numerical computations performed in this work are based on standard results of SAS theory. The specific formulae used are listed below. Theoretical and numerical details will be published separately (Hinde, in press).

1. Density fluctuation autocorrelation function $\gamma(r)$:

autocorrelation function:

$$\gamma(r) = \int_V \Delta\rho(\bar{r}')\Delta\rho(\bar{r}' + \bar{r})\mathrm{d}V' \tag{1.1}$$

density fluctuation:

$$\rho(\underline{\mathbf{r}}) = \bar{\rho} + \Delta\rho(\underline{\mathbf{r}}); \bar{\rho} = \frac{1}{V}\int_V \rho(r)\mathrm{d}r \tag{1.2}$$

where ρ is the electronic density for SAXS and nuclear scattering length density for SANS. Table 2 shows a list of scattering length densities for coals studied in this work.

2. Scattering intensity (scattering cross section) for polycrystalline systems:

$$I(Q) = \frac{\mathrm{d}\sigma}{\mathrm{d}\Omega}(Q) = 4\pi\int_0^\infty r^2\gamma(r)\frac{\sin(Qr)}{Qr}\mathrm{d}r \tag{2.1}$$

3. Traditional expression for the scattering cross section

$$\frac{\mathrm{d}\sigma}{\mathrm{d}\Omega}(Q) = V\overline{\Delta\rho^2}F(Q) \tag{3.1}$$

where the following quantities appear on the right hand side:

$$\text{form factor: } F(Q) = \frac{4\pi}{\overline{\Delta\rho^2}}\int_0^\infty r^2\gamma(r)\frac{\sin(Qr)}{Qr}\mathrm{d}r \tag{3.2}$$

$$\text{contrast: } \overline{\Delta\rho^2} = (\rho_1 - \rho_2)^2\phi(1-\phi) \tag{3.3}$$

and V is the scattering volume, ρ_1 and ρ_2 are the scattering length densities of the coal matrix and the pores, respectively, and ϕ is the volume fraction of pores.

4. Scattering intensity per unit volume for monodisperse spheres of radius r:

$$I(Q) = (\rho_1 - \rho_2)^2\phi(1-\phi)V_rF_{\mathrm{sph}}(Qr) \tag{4.1}$$

where the following quantities appear on the right hand side:

$$\text{contrast: } \overline{\Delta\rho^2} = (\rho_1 - \rho_2)^2\phi(1-\phi) \tag{4.2}$$

porosity: ϕ
volume of individual pore: V_r=(4/3)πr^3

form factor for a sphere of radius r:

$$F_{\mathrm{sph}}(Qr) = \left[3\frac{\sin(Qr) - Qr\cos(Qr)}{(Qr)^3}\right]^2 \tag{4.3}$$

5. Scattering intensity per unit volume for polydisperse spheres of radius r:

$$I(Q) = (\rho_1 - \rho_2)^2\frac{\phi}{\overline{V_r}}\int_{R_{\min}}^{R_{\max}} V_r^2 f(r)F_{\mathrm{sph}}(Qr)\mathrm{d}r \tag{5.1}$$

where $\overline{V_r} = \int_0^\infty V_r f(r)\mathrm{d}r$ is the average pore volume and $f(r)$ the probability density of the pore size distribution.

6. Scattering intensity per unit volume for an arbitrary distribution of spheres of radius r expressed as a histogram:

$$I(Q) = \sum_i IQ_{0i}\frac{\int_{R_{\min}}^{R_{\max}} V_r^2F_{\mathrm{sph}}(Qr)\mathrm{d}r}{(R_{\max,i} - R_{\min,i})} \tag{6.1}$$

where R_{max} and R_{min} are the maximum and minimum pore radii, respectively, and

$$IQ_{0i} = \frac{(\rho_1 - \rho_2)^2 \phi}{\overline{V_r}} f(r_i)(R_{max,i} - R_{min,i}) \qquad (6.2)$$

7. Porosity is the sum of volumes of all pores divided by the sample volume.
8. Specific surface area for probe size r is calculated from the pore size distribution as the sum of surface areas of all pores of radius larger than r divided by the sample volume:

$$\frac{S(r)}{V} = n_v \int_r^{R_{max}} A_r f(r')\mathrm{d}r' \qquad (8.1)$$

where: n_v is the average number of pores per unit volume

$$n_v = \frac{\phi}{\overline{V_r}} = \frac{I(0)}{(\rho_1 - \rho_2)^2} \frac{1}{\overline{V_r^2}} \qquad (8.2)$$

$S(r)$ is the total surface area of pores with radius larger than r and $A_r = 4\pi r^2$.

References

Agamalian, M., Wignall, G.D., Triolo, R., 1997. Optimization of a Bonse–Hart ultra-small-angle neutron scattering facility by elimination of the rocking-curve wings. Journal of Applied Crystallography 30, 345–352.

ASTM, 1985. Annual Book of American Society for Testing and Materials Standards. Sec. 05.05 Gaseous Fuels. Coal and Coke, Philadelphia, PA. 472 pp.

Bale, H.D., Schmidt, P.W., 1984. Small-angle X-ray scattering investigation of submicroscopic porosity with fractal properties. Physical Review Letters 53, 596–599.

Berkowitz, N., 1979. An Introduction to Coal Technology, Fig. 2.1.2, p.28. Academic Press, New York. 345 pp.

Bonse, U., Hart, M., 1965. Small-angle X-ray scattering by spherical particles of polystyrene and polyvinyltoluene. Applied Physics Letters 7, 238–240.

Boreham, C.J., Blevin, J.E., Radlinski, A.P., Trigg, K.R., 2003. Coals as a source of oil and gas: a case study from the Bass Basin, Australia. APPEA Journal, 117–147.

Broseta, D., Barre, L., Vizika, O., Shahidzadeh, N., Guilbaud, J.-P., Lyonnard, S., 2001. Capillary condensation in a fractal porous medium. Physical Review Letters 86 (23), 5313–5316.

Bustin, R.M., Clarkson, C.R., 1998. Geological controls on coalbed methane reservoir capacity and gas content. International Journal of Coal Geology 38, 3–26.

Bustin, R.M., Cameron, A.R., Grieve, D.A., Kalkreuth, W.D., 1985. Coal petrology, its principles, methods, and applications. Short Course Notes – Geological Association of Canada 3 (Victoria, 230 pp.).

Clarkson, C.R., Bustin, R.M., 2000. Binary gas adsorption/desorption isotherms: effect of moisture and coal composition upon carbon dioxide selectivity over methane. International Journal of Coal Geology 42, 241–271.

Cody, G.D., Obeng, M., Thiyagarajan, P., 1997. Structural characterization of the soluble and insoluble fractions of Upper Freeport coal in NMP/CS2 and pyridine using SANS. Energy and Fuels 11, 495–501.

Crosdale, P.J., Beamish, B.B., Valix, M., 1998. Coalbed methane sorption related to coal composition. International Journal of Coal Geology 35, 147–158.

Espinat, D., 1990. Application des techniques de diffusion de la lumiere, des rayons X et des neutrons a l'etude des systemes colloidaux. Revue de l'Institut Francais du Petrole 45 (6), 1–131.

Gentzis, T., 2000. Subsurface sequestration of carbon dioxide—an overview from an Alberta (Canada) perspective. International Journal of Coal Geology 43, 287–305.

Guinier, A., Fournet, G., Walker, C.B., Yudowitch, K.L., 1955. Small-angle Scattering of X-rays. Wiley, New York. 259 pp.

Hainbuchner, M., Villa, M., Kroupa, G., Bruckner, G., Baron, M., Amenitsch, H., Seidl, E., Rauch, H., 2000. The new high resolution ultra small-angle neutron scattering instrument at the high flux reactor in Grenoble. Journal of Applied Crystallography 33, 851–854.

Harris Jr., E.C., Petersen, E.E., 1979. Change of physical characteristics of Roland seam coal with progressive solvent extraction. Fuel 58, 599–602.

Hinde, A.L., 2004. PRINSAS—a Windows-based computer program for the processing and interpretation of small angle scattering data. Journal of Applied Crystallography (in press, The program can be downloaded from the following URL: http://www.ga.gov.au/download/publications.html#marine).

Janowsky, U., 1984. Experimentelle Untersuchungen zum Stroemungs-und Sorptionsverhalten von Wasser und Gasen in Steinkohle und Ableitung eines Porenmodells. Diss., University of Essen, Essen. 144 pp.

Lambard, J., Zemb, Th., 1991. A triple-axis Bonse–Hart camera used for high-resolution small-angle scattering. Journal of Applied Crystallography 24, 555–561.

Levine, J.R., 1993. Coalification: the evolution of coal as source rock and reservoir rock for oil and gas. In: Law, B.E., Rice, D.D. (Eds.), AAPG Studies in Geology, vol. 38, pp. 39–79.

Lin, J.-S., Hendricks, R.W., Harris, L.A., Yust, C.S., 1978. Microporosity and micromineralogy of vitrinite in a bituminous coal. Journal of Applied Crystallography 11, 621–625.

Lindner, P., Zemb, T., 1991. Neutron, X-ray and Light Scattering Elsevier, Amsterdam.

Littke, R., Leythaeuser, D., 1993. Migration of oil and gas in coals. In: Law, B.E., Rice, D.D. (Eds.), AAPG Studies in Geology, vol. 38, pp. 219–236.

Mastalerz, M., Bustin, R.M., 1993. Variation in maceral chemistry within and between coals of varying rank: an electron micro-

probe and micro-FTIR investigation. Journal of Microscopy 171 (Part 2), 153–166.

Mildner, D.F.R., Hall, P.L., 1986. Small-angle scattering from porous solids with fractal geometry. J. Phys., D, Appl. Phys. 19, 1535–1545.

Pfeifer, P., Avnir, D., 1983. Chemistry in noninteger dimensions between two and three. I. Fractal theory of heterogeneous surfaces. Journal of Chemical Physics 79, 3558–3565.

Radlinski, A.P., Hinde, A.L., 2001. Applications of small angle neutron scattering and small angle X-ray scattering to petroleum geology. Proceedings of the ESRF/ILL Joint Workshop on Environmental Studies Using Neutron and Synchrotron Facilities, Grenoble, France, February 20–21, 2001. 11 pp.

Radlinski, A.P., Hinde, A.L., 2002. Small angle neutron scattering and petroleum geology. Neutron News 13 (2), 10–14.

Radlinski, A.P., Radlinska, E.Z., 1999. The microstructure of pore space in coals of different rank: a small angle scattering and SEM study. In: Mastalerz, M., Glikson, M., Golding, S.D. (Eds.), Coalbed Methane: Scientific, Environmental and Economic Evaluation. Kluwer Scientific, Dodrecht, pp. 329–365.

Radlinski, A.P., Boreham, C.J, Wignall, G.D., Lin, J.-S., 1996. Microstructural evolution of source rocks during hydrocarbon generation: a small-angle scattering study. Physical Review B 53, 14152–14160.

Radlinski, A.P., Radlinska, E.Z., Agamalian, M., Wignall, G.D., Lindner, P., Randl, O.G., 1999. Fractal geometry of rocks. Physical Review Letters 82, 3078–3081.

Radlinski, A.P., Radlinska, E.Z., Agamalian, M., Wignall, G.D., Lindner, P., Randl, O.G., 2000a. The fractal microstructure of ancient sedimentary rocks. Journal of Applied Crystallography 33, 860–862.

Radlinski, A.P., Boreham, C.J., Lindner, P., Randl, O.G., Wignall, G.D., Hope, J.M., 2000b. Small angle neutron scattering signature of oil generation in artificially and naturally matured hydrocarbon source rocks. Organic Geochemistry 31, 1–14.

Radlinski, A.P., Mastalerz, M., Hinde, A., Hainbuchner, M., Rauch, H., Baron, M., Lin, J.S., Fan, L., Thiyagarajan, P., 2001. Noninvasive measurements of pore size distribution in coal pellets using X-ray and neutron techniques. Proceedings of the 2001 International Coalbed Methane Symposium, Tuscaloosa, AL, 2001, Paper No. 0118, pp. 163–175.

Russell, T.P., Lin, J.S., Spooner, S., Wignall, G.D., 1988. Intercalibration of small-angle X-ray and neutron scattering data. Journal of Applied Crystallography 21, 629–638.

Schmidt, P.W., 1982. Interpretation of small-angel scattering curves proportional to a negative power of the scattering vector. Journal of Applied Crystallography 15, 567–569.

Thiyagarayan, P., Urban, V., Littrell, K., Ku, C., Wozniak, D.G., Belch, H., Vitt, R., Toeller, J., Leach, D., Haumann, J.R., Ostrowski, G.E., Donley, L.I., Hammonds, J., Carpenter, J.M., Crawford, R.K., 1998. The performance of the small-angle diffractometer, SAND at IPNS″, ICANS-XIV. 14th Meeting of the International Collaboration on Advanced Neutron Sources, June 14–19 1998, Starved Rock Lodge, Utica, Illinois.

Winans, R.E., Thiyagarajan, P., 1988. Characterization of solvent-swollen coal by SANS. Energy and Fuels 2, 356–358.

Wong, P.-Z., Howard, J., Lin, J.-S., 1986. Surface roughening and the fractal nature of rocks. Physical Review Letters 57, 637–640.

Yee, D., Seidle, J.P., Hanson, W.B., 1993. Gas sorption on coal and measurement of gas content. In: Law, B.E., Rice, D.D. (Eds.), AAPG Studies in Geology, vol. 38, pp. 203–218.